

An efficient computation of geometric entanglement for two-dimensional quantum lattice systems

Hong-Lei Wang, Qian-Qian Shi, Sheng-Hao Li, and Huan-Qiang Zhou¹

¹*Centre for Modern Physics and Department of Physics,
Chongqing University, Chongqing 400044, The People's Republic of China*

The geometric entanglement per lattice site, as a holistic measure of the multipartite entanglement, serves as a universal marker to detect quantum phase transitions in quantum many-body systems. However, it is very difficult to compute the geometric entanglement due to the fact that it involves a complicated optimization over all the possible separable states. In this paper, we propose a systematic method to efficiently compute the geometric entanglement per lattice site for quantum many-body lattice systems in two spatial dimensions in the context of a newly-developed tensor network algorithm based on an infinite projected entangled pair state representation. It is tested for quantum Ising model in a transverse magnetic field and anisotropic spin 1/2 anti-ferromagnetic XYX model in an external magnetic field on an infinite-size square lattice. In addition, the geometric entanglement per lattice site is able to detect the so-called factorizing field. Our results are in a quantitative agreement with Quantum Monte Carlo simulations.

PACS numbers: 03.67.-a, 03.65.Ud, 03.67.Hk

Introduction. The geometrical entanglement is a measure of the multipartite entanglement present in a quantum state wave function. It quantifies the distance between a given quantum state wave function and the closest separable state [1, 2]. Remarkably, it serves as an alternative marker [2–4] to locate critical points for quantum many-body lattice systems undergoing quantum phase transitions (QPTs) [5, 6]. In addition, an intriguing connection to both the Renormalization Group and Conformal Field Theory has been unveiled for quantum many-body lattice systems in one spatial dimension [7–9]. Furthermore, recent numerical simulations [8] established a universal finite-size correction to the geometric entanglement for the critical XXZ and transverse quantum Ising chains, which in turn is related with the celebrated Affleck-Ludwig g factors [9, 10]. Therefore, the geometrical entanglement offers a powerful tool to investigate quantum criticality in quantum many-body lattice systems. However, almost all studies have been restricted to quantum many-body lattice systems in one spatial dimension, with an exception [11], in which the geometrical entanglement is exploited to study QPTs for quantum many-body lattice systems in two spatial dimensions. This is mainly due to the fact that it is very difficult to compute the geometrical entanglement, because it involves a complicated optimization over all the possible separable states.

On the other hand, significant progress has been made to develop efficient numerical algorithms to simulate quantum many-body lattice systems in the context of the tensor network representations [12–21]. The algorithms have been successfully exploited to compute the ground-state fidelity per lattice site [22–26], a universal marker to detect QPTs, for quantum many-body lattice systems. Indeed, the ground-state fidelity per lattice site is closely related to the geometrical entanglement. Therefore, it is natural to expect that there should be an efficient way to compute the geometrical entanglement in the context of the tensor network algorithms. Actually, this has been achieved for quantum many-body lattice systems with the periodic boundary conditions in one spatial dimension

[10] in the context of the matrix product state representation.

In the present work, we propose a systematic method to efficiently compute the geometric entanglement per lattice site for quantum many-body lattice systems in two spatial dimensions in the context of a newly-developed tensor network algorithm based on an infinite projected entangled pair state (iPEPS) representation. It is exploited to evaluate the geometric entanglement per lattice site for quantum Ising model in a transverse magnetic field and anisotropic spin 1/2 anti-ferromagnetic XYX model in an external magnetic field on an infinite-size square lattice, which enables us to identify their critical points. In addition, the geometric entanglement per lattice site is able to detect the so-called factorizing field. Our results are in a quantitative agreement with Quantum Monte Carlo simulations.

The geometric entanglement per lattice site. For a pure quantum state $|\psi\rangle$ with N parties, the geometric entanglement, as a global measure of the multipartite entanglement, quantifies the deviation from the closest separable state $|\phi\rangle$. Mathematically, the geometric entanglement [8, 9] $E(|\psi\rangle)$ for an N -partite quantum state $|\psi\rangle$ is expressed as:

$$E(|\psi\rangle) = -\log_2 \Lambda_{\max}^2, \quad (1)$$

where Λ_{\max} is the maximum fidelity between $|\psi\rangle$ and all the possible separable and normalized state $|\phi\rangle$, with

$$\Lambda_{\max} = \max_{|\phi\rangle} |\langle\psi|\phi\rangle|. \quad (2)$$

Then, the geometric entanglement per party $\mathcal{E}_N(|\psi\rangle)$ is defined as:

$$\mathcal{E}_N(|\psi\rangle) = N^{-1}E(|\psi\rangle). \quad (3)$$

It corresponds to the maximum fidelity per party λ_N^{\max} , where

$$\lambda_N^{\max} = \sqrt[N]{\Lambda_{\max}}, \quad (4a)$$

or, equivalently,

$$\mathcal{E}_N(|\psi\rangle) = -\log_2 (\lambda_N^{\max})^2. \quad (4b)$$

For our purpose, we shall consider a quantum many-body system on an infinite-size lattice in two spatial dimensions, which undergoes a QPT at a critical point in the thermodynamic limit. In this situation, each lattice site constitutes a party, thus the geometric entanglement per party becomes the geometric entanglement per lattice site, which is well defined even in the thermodynamic limit ($N \rightarrow \infty$), since the contribution to fidelity from each party (site) is multiplicative.

The infinite projected entangled pair state algorithm. Our aim is to compute the geometric entanglement per lattice site for a quantum many-body lattice system on an infinite-size square lattice in the context of the iPEPS algorithm [14]. Suppose we consider a system characterized by a translation-invariant Hamiltonian H with the nearest-neighbor interactions: $H = \sum_{\langle ij \rangle} h_{\langle ij \rangle}$, with $h_{\langle ij \rangle}$ being the Hamiltonian density. Assume that a quantum wave function $|\psi\rangle$ is translation-invariant under two-site shifts, then one only needs two five-index tensors A_{lrud}^s and B_{lrud}^s to express the iPEPS representation. Here, each tensor is labeled by one physical index s and four bond indices l, r, u and d , as shown in Fig.1(i). Note that the physical index s runs over $1, \dots, \mathfrak{d}$, and each bond index takes $1, \dots, D$, with \mathfrak{d} being the physical dimension, and D the bond dimension. Therefore, it is convenient to choose a 2×2 plaquette as the unit cell (cf. Fig.1(ii)). The ground-state wave function is well approximated by $|\psi_\tau\rangle$, which is obtained by performing an imaginary time evolution [14] from an initial state $|\psi_0\rangle$, with $|\psi_\tau\rangle = e^{-H\tau}|\psi_0\rangle/\|e^{-H\tau}|\psi_0\rangle\|$ [14], as long as τ is large enough.

A key ingredient of the iPEPS algorithm is to take advantage of the Trotter-Suzuki decomposition that allows to reduce the (imaginary) time evolution operator $e^{-H\delta\tau}$ over a time slice $\delta\tau$ into the product of a series of two-site operators, where the imaginary time interval τ is divided into M slices: $\tau = M\delta\tau$. Therefore, the original global optimization problem becomes a local two-site optimization problem. With an efficient contraction scheme available to compute the effective environment for a pair of the tensors A_{lrud}^s and B_{lrud}^s [14], one is able to update the tensors A_{lrud}^s and B_{lrud}^s . Performing this procedure until the energy per lattice site converges, the ground-state wave function is produced in the iPEPS representation.

Efficient computation of the geometric entanglement in the iPEPS representation. Once the iPEPS representation for the ground-state wave function is generated, we are ready to evaluate the geometric entanglement per lattice site. First, we need to compute the fidelity between the ground-state wave function and a separable state. The latter is represented in terms of one-index tensors \tilde{A}^s and \tilde{B}^s . To this end, we form a reduced four-index tensor a_{lrud} from the five-index tensor A_{lrud}^s and a one-index tensor \tilde{A}^s , as depicted in Fig. 1 (iii). As such, the fidelity is represented as a tensor network in terms of the reduced tensors a_{lrud} and b_{lrud} (cf. Fig. 1 (iv)). The tensor network may be contracted as follows. First, form the one-dimensional transfer matrix E_1 , consisting of two consecutive rows of the tensors in the checkerboard tensor network. This is highlighted in Fig. 1 (vi) with two dash lines. Second, compute the dominant eigenvectors of the transfer matrix E_1 ,

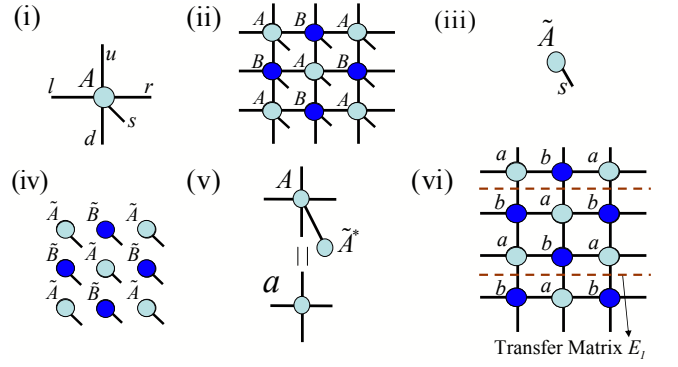


FIG. 1: (color online) (i) A five-index tensor A_{lrud}^s labeled by one physical index s and four bond indices l, r, u and d . (ii) The iPEPS representation of a wave function in two-dimensional square lattice. Copies of the tensors A_{lrud}^s and B_{lrud}^s are connected through four types of bonds. (iii) A one-index tensor \tilde{A}^s labeled by one physical index s . (iv) The iPEPS representation of a separable state in two-dimensional square lattice. (v) A reduced four-index tensor a_{lrud} from a five-index tensor A_{lrud}^s and a one-index \tilde{A}^s . (vi) The tensor network representation for the fidelity between a quantum wave function (describe by A_{lrud}^s and B_{lrud}^s) and a separable state (described by \tilde{A}^s and \tilde{B}^s), consisting of the reduced tensors a_{lrud} and b_{lrud} .

corresponding to the dominant eigenvalue. This can be done, following a procedure described in Ref. [16]. Here, the dominant eigenvectors are represented in the infinite matrix product states. Third, choose the zero-dimensional transfer matrix E_0 , and compute its dominant left and right eigenvectors, V_L and V_R . This may be achieved by means of the Lanczos method. In addition, one also needs to compute the norms of the ground-state wave function $|\psi\rangle$ and a separable state $|\phi\rangle$ from their iPEPS representations. Putting everything together, we are able to get the fidelity per unit cell between the ground state $|\psi\rangle$ and a separable state $|\phi\rangle$:

$$\lambda = \frac{|\eta_{\langle\phi|\psi\rangle}|}{\sqrt{\eta_{\langle\psi|\psi\rangle}\eta_{\langle\phi|\phi\rangle}}}, \quad (5)$$

where $\eta_{\langle\phi|\psi\rangle}$, $\eta_{\langle\phi|\phi\rangle}$ and $\eta_{\langle\psi|\psi\rangle}$ are, respectively, the dominant eigenvalue of the zero-dimensional transfer matrix E_0 for the iPEPS representation of $\langle\phi|\psi\rangle$, $\langle\psi|\psi\rangle$ and $\langle\phi|\phi\rangle$. Then we proceed to compute the geometric entanglement per lattice site, which involves the optimization over all the separable states. For our purpose, we define $F = \lambda^2$. The optimization amounts to computing the logarithmic derivative of F with respect to \tilde{A}^s , which is expressed as

$$G \equiv \frac{\partial \ln F}{\partial \tilde{A}^s} = \frac{1}{\eta_{\langle\phi|\psi\rangle}} \frac{\partial \eta_{\langle\phi|\psi\rangle}}{\partial \tilde{A}^s} - \frac{1}{\eta_{\langle\phi|\phi\rangle}} \frac{\partial \eta_{\langle\phi|\phi\rangle}}{\partial \tilde{A}^s}. \quad (6)$$

Therefore, the problem reduces to the computation of G in the context of the tensor network representation. First, note that a pictorial representation of the derivative $\partial a_{lrud}/\partial \tilde{A}^s$ of the four-index tensor a_{lrud} with respect to \tilde{A}^s is shown in Fig. 2 (ii), which is nothing but the five-index tensor A_{lrud}^s . Similarly, we may define the derivative of the four-index tensor b_{lrud} with respect to \tilde{B}^s . Then, we are able to represent

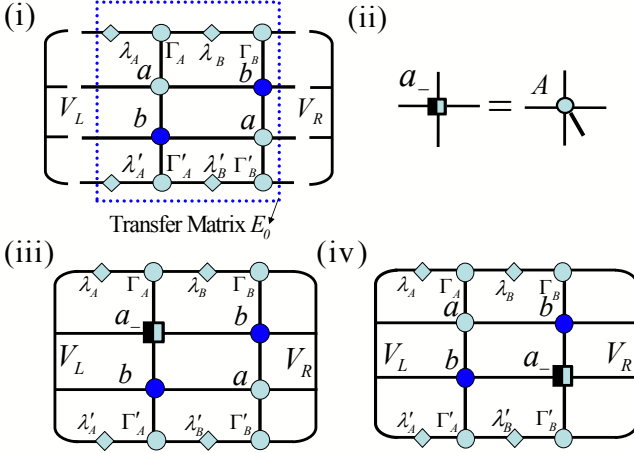


FIG. 2: (color online) The gradient of the fidelity between a given ground-state wave function $|\psi\rangle$ and a separable state $|\phi\rangle$ in the iPEPS representation. (i): The zero-dimensional transfer matrix E_0 and its dominant eigenvectors V_L and V_R . Here, the infinite matrix product state representation of the dominant eigenvectors for the one-dimensional transfer matrix E_1 follows from Ref. [16], and V_L and V_R may be evaluated from the Lanczos method. The contraction of the entire tensor network is the dominant eigenvalue $\eta_{\langle\phi|\psi\rangle}$ of the zero-dimensional transfer matrix E_0 for $\langle\phi|\psi\rangle$. (ii): A half-filled square denotes a_- , the derivative of the four-index tensor a_{lrud} with respect to \tilde{A}^{s*} , which is nothing but the five-index tensor A_{lrud}^s . Similarly, we may define b_- , the derivative of the four-index tensor b_{lrud} with respect to \tilde{B}^{s*} . (iii) and (iv): The pictorial representation of the contributions to the derivative of $\eta_{\langle\phi|\psi\rangle}$ with respect to \tilde{A}^{s*} , with different relative positions between filled circles and half-filled squares.

the contributions to the derivative of $\eta_{\langle\phi|\psi\rangle}$ with respect to \tilde{A}^{s*} in Fig. 2 (iii) and (iv). In our scheme, we update the real and imaginary parts of \tilde{A}^s separately:

$$\Re(\tilde{A}^s) = \Re(\tilde{A}^s) + \delta \Re(G)^s, \quad (7a)$$

and

$$\Im(\tilde{A}^s) = \Im(\tilde{A}^s) + \delta \Im(G)^s. \quad (7b)$$

Here, $\delta \in [0, 1)$ is the step size in the parameter space, which is tuned to be decreasing during the optimization process. In addition, we have normalized the real and imaginary parts of the gradient G so that their respective largest entries are unity. The procedure to update the tensor \tilde{B}^s is the same. If the fidelity per unit cell converges, then the closest separable state $|\phi\rangle$ is achieved, thus the geometric entanglement per lattice site for the ground-state wave function $|\psi\rangle$ follows.

The models. As a test, we simulate two typical quantum many-body lattice systems on an infinite-size square lattice in two spatial dimensions. The first model is quantum Ising model in a transverse magnetic field. The Hamiltonian takes the form,

$$H = - \sum_{\langle i,j \rangle} S_x^{[i]} S_x^{[j]} - h \sum_i S_z^{[i]}, \quad (8)$$

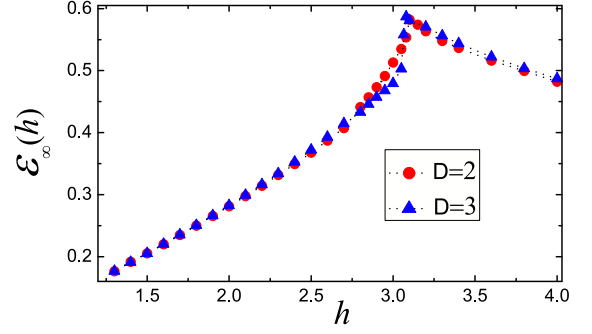


FIG. 3: (color online) The geometric entanglement per lattice site $\mathcal{E}_\infty(h)$ as a function of the transverse magnetic field strength h for quantum transverse Ising model on an infinite-size square lattice in two spatial dimensions. The data are presented for both the truncation dimension $D = 2$ and $D = 3$. The cusp in the $\mathcal{E}_\infty(h)$ curve reflects a drastic change of the multipartite entanglement around a critical point: $h_c = 3.1$ for $D = 2$ and $h_c = 3.08$ for $D = 3$. Quantum Monte Carlo simulation indicates a critical point at $h_{\text{QMC}} \approx 3.044$.

where $S_\alpha^{[j]}(\alpha = x, z)$ are the spin-1/2 Pauli operators at lattice site j , h is a transverse magnetic field, and $\langle i, j \rangle$ runs over all the possible pairs of the nearest neighbors on a square lattice. Quantum Monte Carlo simulation predicts a critical point at $h_{\text{QMC}} \sim 3.044$ [27].

The second model is quantum anti-ferromagnetic XYX model in an external magnetic field. The Hamiltonian is written as,

$$H = J \sum_{\langle i,j \rangle} (S_x^{[i]} S_x^{[j]} + \Delta_y S_y^{[i]} S_y^{[j]} + S_z^{[i]} S_z^{[j]}) + h \sum_i S_z^{[i]}, \quad (9)$$

where $S_\alpha^{[j]}(\alpha = x, y, z)$ are the spin-1/2 Pauli operators at lattice site j , $J > 0$ is the exchange coupling, $\langle i, j \rangle$ runs over all the possible pairs of the nearest neighbors on a square lattice, and h is an external magnetic field. Note that $\Delta_y < 1$ and $\Delta_y > 1$ correspond to the easy-plane and easy-axis behaviors, respectively. Here, we focus on $\Delta_y = 0.25$. In this case, the model is known to undergo a continuous QPT in the same universality class as the transverse Ising model [28].

Simulation results. We plot the geometric entanglement per lattice site for quantum Ising model in a transverse field, with the field strength h as the control parameter, in Fig. 3. There is a cusp at $h_c = 3.10$ for the truncation dimension $D = 2$ and $h_c = 3.08$ for the truncation dimension $D = 3$, respectively, on the curve of the geometric entanglement as a function of the transverse field h . On both sides of the cusp, it is continuous. This implies that a continuous QPT occurs at h_c .

In Fig. 4, the geometric entanglement per lattice site for quantum XYX model in an external magnetic field h , with $\Delta_y = 0.25$, is plotted. Here, the external magnetic field strength h is chosen as the control parameter. A cusp occurs as h varies across a critical point h_c : $h_c = 3.49$ for the truncation dimension $D = 2$ and $h_c = 3.485$ for the truncation dimension $D = 3$, respectively. On both sides of the cusp, the geometric entanglement per lattice site is continuous, which implies that

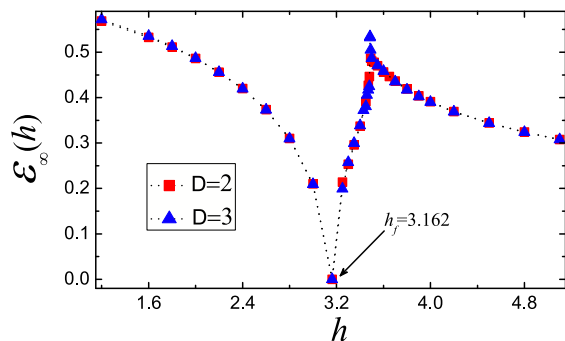


FIG. 4: (color online) The geometric entanglement per lattice site $\mathcal{E}_\infty(h)$ as a function of the applied external magnetic field h for quantum XYX model on an infinite-size square lattice in two spatial dimensions, with $\Delta_y = 0.25$. The data are presented for both $D = 2$ and $D = 3$. The factorizing field, at which the geometric entanglement per lattice site vanishes, is indicated by an arrow labeled by h_f around 3.162. Above the factorizing field h_f , a sharp increase of $\mathcal{E}_\infty(h)$ reflects a rapid increase of the multipartite entanglement around a critical point: $h_c = 3.49$ for $D = 2$ and $h_c = 3.485$ for $D = 3$.

the model undergoes a continuous QPT at h_c .

Notice that, only a small shift is observed for h_c , with increasing of the truncation dimension, for both models. This indicates that the iPEPS algorithm captures many-body physics for both models, with a small truncation dimension, as already observed before [14, 23, 26]. Our simulation results are in a quantitative agreement with Quantum Monte Carlo simulation for quantum Ising model in a transverse field [27] and for quantum XYX model in an external magnetic field h , with $\Delta_y = 0.25$ [28]. In addition, our simulation indicates that a factorizing field h_f occurs at $h_f = 0$ and $h_f = 3.162$, respectively, for quantum Ising model in a transverse field and for quantum XYX model in an external magnetic field h , with $\Delta_y = 0.25$, thus reproducing the exact results. We stress that a factorizing field h_f is identified from $\mathcal{E}_\infty(h_f) = 0$.

Conclusions. In this paper, we have demonstrated how to efficiently compute the geometric entanglement per lattice site, by optimizing over all the possible separable states, in the context of the tensor network algorithm based on the iPEPS representation. The geometric entanglement per lattice site, as a holistic measure of the multipartite entanglement, serves as a universal marker to locate critical points underlying quantum many-body lattice systems. Our method is tested for both quantum Ising model in a transverse magnetic field and an anisotropic spin 1/2 anti-ferromagnetic XYX model in an external magnetic field on an infinite-size square lattice, succeeded in identifying both the critical points and factorizing fields. We expect that, with the developments of powerful tensor network algorithms, the geometric entanglement per lattice site adds a new route to explore quantum criticality for quantum many-body lattice systems in condensed matter physics.

Acknowledgements. The work is partially supported by

the National Natural Science Foundation of China (Grant No: 10874252). HLW, QQS, and SHL are supported by the Fundamental Research Funds for the Central Universities (Project No. CDJXS11102214) and by Chongqing University Postgraduates' Science and Innovation Fund (Project No.: 200911C1A0060322).

-
- [1] H. Barnum and N. Linden, *J. Phys. A: Math. Gen.* **34**, 6787 (2001).
 - [2] T.-C. Wei and P. M. Goldbart, *Phys. Rev. A* **68**, 042307 (2003); T.-C. Wei, D. Das, S. Mukhopadhyay, S. Vishveshwara, and P.M. Goldbart, *Phys. Rev. A* **71**, 060305 (2005).
 - [3] R. Orús and T.-C. Wei, *Phys. Rev. B* **82**, 155120 (2010).
 - [4] R. Orús, T.-C. Wei, and H.-H. Tu, arXiv:1010.5029; R. Orús and T.-C. Wei, arXiv:1006.5584.
 - [5] S. Sachdev, *Quantum Phase Transitions*, Cambridge University Press, 1999, Cambridge.
 - [6] X.-G. Wen, *Quantum Field Theory of Many-Body Systems*, Oxford University Press, 2004, Oxford.
 - [7] A. Botero and B. Reznik, arXiv:0708.3391; R. Orús, *Phys. Rev. Lett.* **100**, 130502 (2008).
 - [8] Q.-Q. Shi, R. Orús, J. O. Fjærestad, and H.-Q. Zhou, *New J. Phys.* **12**, 025008 (2010).
 - [9] J.-M. Stéphan, G. Misguich, and F. Alet, *Phys. Rev. B* **82**, 180406R (2010).
 - [10] B.-Q. Hu, X.-J. Liu, J.-H. Liu, and H.-Q. Zhou, preprint.
 - [11] C.-Y. Huang and F.-L. Lin, *Phys. Rev. A* **81**, 032304 (2010).
 - [12] F. Verstraete, D. Porras, and J.I. Cirac, *Phys. Rev. Lett.* **93**, 227205 (2004). F. Verstraete and J.I. Cirac, arXiv:cond-mat/0407066; V. Murg, F. Verstraete, and J.I. Cirac, *Phys. Rev. A* **75**, 033605 (2007).
 - [13] G. Vidal, *Phys. Rev. Lett.* **91**, 147902 (2003); G. Vidal, *Phys. Rev. Lett.* **93**, 040502 (2004). G. Vidal, *Phys. Rev. Lett.* **98**, 070201 (2007).
 - [14] J. Jordan, R. Orús, G. Vidal, F. Verstraete, and J. I. Cirac, *Phys. Rev. Lett.* **101**, 250602 (2008).
 - [15] B. Bauer, G. Vidal, and M. Troyer, *J. Stat. Mech.* (2009) P09006.
 - [16] R. Orús and G. Vidal, *Phys. Rev. B* **78**, 155117 (2009).
 - [17] P. Pippin, S. R. White, and H. G. Evertz, *Phys. Rev. B* **81**, 081103(R) (2010).
 - [18] Q.-Q. Shi and H.-Q. Zhou, *J. Phys. A: Math. Theor.* **42** 272002 (2009).
 - [19] J. Haegeman, J. I. Cirac, and T. J. Osborne, I. Pižorn, H. Verschelde, and F. Verstraete, arXiv:1103.0936.
 - [20] H. C. Jiang, Z. Y. Weng, and T. Xiang, *Phys. Rev. Lett.* **101**, 090603 (2008).
 - [21] L. Wang, Y.-J. Kao, and A.W. Sandvik, *Phys. Rev. E* **83**, 056703 (2011).
 - [22] H.-Q. Zhou and J.P. Barjaktarevič, *J. Phys. A: Math. Theor.* **41** 412001 (2008); H.-Q. Zhou, J.-H. Zhao, and B. Li, *J. Phys. A: Math. Theor.* **41** 492002 (2008).
 - [23] H.-Q. Zhou, R. Orús, and G. Vidal, *Phys. Rev. Lett.* **100**, 080602 (2008).
 - [24] J.-H. Zhao, H.-L. Wang, B. Li, and H.-Q. Zhou, arXiv:0902.1669. *Phys. Rev. E* **82**, 061127 (2010).
 - [25] H.-L. Wang, J.-H. Zhao, B. Li, and H.-Q. Zhou, arXiv:0902.1670.
 - [26] B. Li, S.-H. Li, and H.-Q. Zhou, *Phys. Rev. E* **79**, 060101(R) (2009).

- [27] H.W.J. Blote and Y. Deng, Phys. Rev. E **66**, 066110 (2002).
[28] T. Roscilde *et. al.*, Phys. Rev. Lett. **94**, 147208 (2005).